Publishing Excellence
Inspiring Progress

ISSN: 0000-0000 www.aristonpubs.com/journal/science-of-optics-and-photonics https://doi.org/10.69626/sop.2026.0019

RESEARCH ARTICLE

# MATLAB Simulation based Study of a Lossy Mode Resonance Sensor Design with Improved Detection Accuracy

**Arun Uniyal[1*], Vipin Sharma[2], Priyanka Dobhal Uniyal[3], D.K. Dwivedi[4]**

**ABSTRACT:** Lossy Mode Resonance (LMR) has become an attractive approach for optical sensing due to its high sensitivity toward changes in the refractive index of various dielectric, semiconductor, or transparent conductive oxide (TCO) materials. A novel type of prism-coupled multi-layer lossy mode resonance sensor (Prism / Cytop / ITO / $TiO_2$ / Sensing Medium) is designed and simulated by use of Transfer Matrix Method (TMM), which was written in MATLAB under angular interrogation. Indium Tin Oxide (ITO) is used as the lossy mode resonance support layer, while cytop and $TiO_2$ layers were added to improve optical coupling, modal confinement and resonance performance. The effects of TM and TE polarizations, cytop thickness, ITO thickness and $TiO_2$ thickness on reflectance spectra are examined thoroughly. The sensor was tested for refractive index values ranging from 1.33 – 1.41 at a wavelength of 633 nm. It can be seen that the TE polarization mode shows a narrower resonant peak with smaller minima in reflection spectrum and better detection accuracy than TM polarization mode. The optimization of multi-layered structure show that a 5nm thick $TiO_2$ layer offers the strongest and most defined LMR effect and therefore chosen as the best configuration.

**Keywords:** Detection Accuracy; Refractive Index; Lossy Mode Resonance; Transfer Matrix Method; Cytop.

**Received: 07 May 2026; Revised: 23 July 2026; Accepted: 29 July 2026; Published Online: 29 August 2026**

## 1. INTRODUCTION

The fast and precise determination of fluctuations in the refractive index (RI), of biological, chemical, or environmental mediums is critical for developing new and advanced optical sensing systems. Because they offer the advantages of being highly sensitive; non-labelled; compact; resistant to electromagnetic interference and potentially capable of continuous measurement, there is currently much interest in optical sensing devices [1]. For example, Surface Plasmon Resonance (SPR) is one of several optical sensing mechanisms that have received extensive investigation for both chemical and bio-sensing applications due to its ability to measure small RI variations in analyte mediums [2, 3]. However, traditional SPR based sensors typically consist of at least one layer made from a noble metal [4, 5] and therefore suffer from limitations including higher costs associated with the materials used, increased complexities when manufacturing these devices and reduced design flexibility in terms of selection of sensing-layer materials. Therefore, researchers have been interested in exploring other resonance mechanisms that can provide similar levels of sensitivity as SPR but which also allow for the use of wider ranges of materials when designing optical sensors. Lossy mode resonance (LMR), a recently discovered optical phenomena, may represent a novel method for obtaining highly sensitive refractive index

[1] Department of Electronics Communication Engineering, Institute of Technology Gopeshwar, Chamoli, Uttarakhand 246424, India
[2] Department of Physics, Rana Pratap Post Graduate College, Sultanpur, Uttar Pradesh 228001, India
[3] District Project Office, Samagra Shiksha, Chamoli, Uttarakhand 246401, India
[4] Department of Physics and Material Science, Madan Mohan Malaviya University of Technology, Gorakhpur, 273010, India

[*] Author to whom correspondence should be addressed: arunavenue@gmail.com (A. Uniyal)

© Ariston Publications 2026. All rights reserved.

sensing [6, 7]. LMR arises from the real part of the permittivity of thin absorbing or lossy films being greater than the imaginary part of the permittivity of these films, such that lossy guided modes are excited at the interface between the coating layer and the surrounding medium [8, 9]. As opposed to SPR, which is primarily associated with the negative real permittivity of noble metals, LMR can be supported by dielectric, semiconductor, and transparent conductive oxide materials exhibiting suitable optical properties [10, 11]. Therefore, LMR offers considerable freedom in the selection and engineering of functional sensing layers. Additionally, LMR may exhibit narrow resonant features and a pronounced shift in resonance position in response to small changes in the surrounding refractive index, making it attractive for high-resolution sensing applications.

Del Villar et al. [12] created LMR for refractive index (RI) measurement in 2010, no one knew that LMR existed for optical sensing purposes. The first RI sensor made from LMR and RI measurements of water-glycerine mixtures was made by using two different thicknesses of ITO film (115nm and 220nm). It demonstrated sensitivities for the RI of the solutions as follows; 1617.4 nm/RIU and 2952.6nm/RIU, respectively. At the same time as Del Villar's research, Zamarreno et al. published the development of an ITO coated optical fiber refractometer that could measure the refractive indices independently of the length of the refracting area. On average, they found a sensitivity of 3125 nm/RIU for the refractometer which is comparable to that of SPR sensors [13]. In addition, researchers have used the LMR effect for RH sensing and developed a RH sensor whose RH sensitivity can be changed depending on the ratio of deposited PAH/PAA layers. Sensitivity comparison of tuned and non-tuned RH sensors has been conducted. Also, VOC sensing was done using an organometallic compound sensitive to VOCs and a novel LMR-based vapor sensor for VOCs was developed. A biosensor for diagnosing celiac disease has also been designed utilizing an LMR-sensing principle. Moreover, theoretical discussions of exposing LMR to temperature sensing were discussed previously [14].

SPRs and LMRs can be achieved using either thin-film-coated optical fiber or thin-film-coated optical prism. However, the conditions that lead to the creation of an LMR will differ significantly from the conditions needed to create a SPR. A SPR is produced as soon as the thin film has a negative real component that is larger than both its own imaginary component and the permittivity of the material it is surrounded with. Conversely, if the thin film has a positive real component which is larger than both its own imaginary component and the material it surrounds, then the LMR is produced [15].

Thin Film Material Permittivity:

$$\varepsilon = \varepsilon_r + i\varepsilon_i \tag{1}$$

Where, $\varepsilon_r$ = real part of permittivity; $\varepsilon_i$ = Imaginary component of permittivity

Indium tin oxide (ITO), are among the most studied material for the excitation of LMR due to its optical and electrical characteristics which include a controllable amount of charge carriers, as well as suitable permittivity [13]. The ability to tailor the LMR response even further may also be realized through variations in the coatings' thickness and optical properties. A means to add additional constraints on both the modal properties of the waveguide and the degree of spatial confinement of the electromagnetic fields within the structure can be provided through the integration of high refractive index dielectrics. Among those considered to be candidates for such dielectrics is titanium dioxide ($TiO_2$), since it has a high refractive index, low optical absorption in the visible spectral range, good chemical stability, and will easily integrate into thin film optical structures [16].

The selection of the substrate and the coupling configuration will have an impact on producing both high sensitivity and a well-defined LMR response. For this research study, we have used a prism coupled configuration and have utilized cytop as an intermediate low refractive index layer. Cytop has a low refractive index that results in low optical loss and thus supports the generation of the desired LMR mode by providing control over the optical coupling conditions [17].

The proposed multi-layered arrangement composed of; a 2S2G Prism / Cytop / ITO / $TiO_2$ / Sensing-Medium layer-structure has been numerically examined utilizing the Transfer Matrix Method (TMM) with respect to Angular Interrogation. A systematic investigation was performed in order to determine the optimal thickness for the $TiO_2$ that would yield the maximum Resonance Characteristics.

## 2. DESIGN CONFIGURATION

The schematic of the proposed prism-coupled LMR sensor is simulated to be able to measure the RI of biochemical solutions with enhanced performance shown by Figure 1.

 © Ariston Publications 2026. All rights reserved.

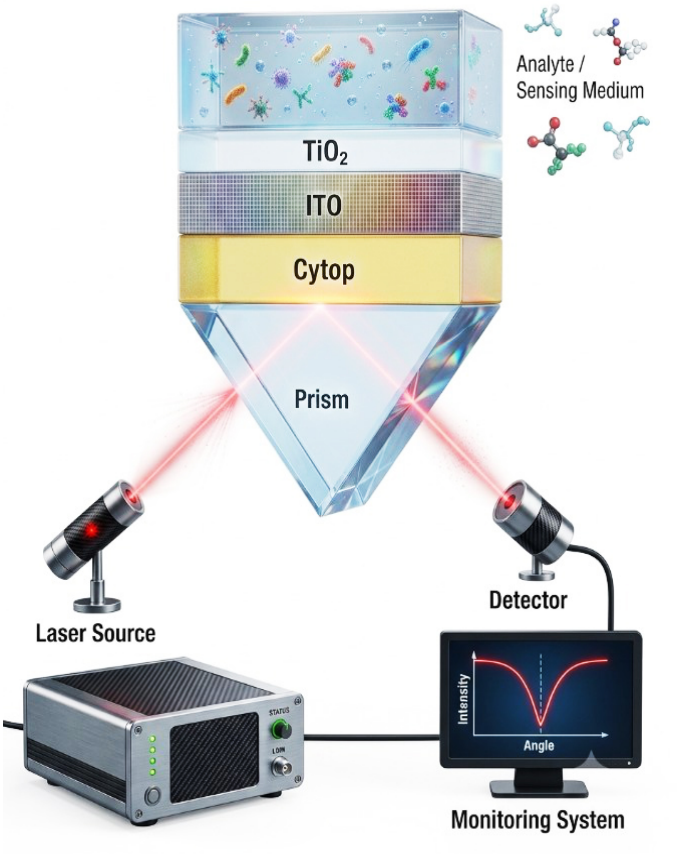



**Fig. 1.** Sensor design of the current LMR sensor.

A laser emits incident light that is then directed through the prism to be totally internally reflected over a defined angle, which transfers the optical energy into the lossy guided modes in the multi layered thin-film stack consisting of a low-index cytop buffer layer, ITO LMR-support film, and high-index titanium dioxide $TiO_2$ protective top coat. Light interacting with the analyte solution above the $TiO_2$ surface causes the detector to capture reflectivity dip characteristics of the system. Through angled displacement measurements, when target biological and chemical analytes are introduced and cause the local refractive index to change, the LMR condition shifts; thus, allowing real-time quantitative monitoring of binding events and concentration changes in the solution. The RI and thickness values used in this simulation LMR study at 633nm is tabulated in Table 1.

### 2.1 N-layer Transfer Matrix Method

The reflectance spectrum and resonance angle were computed using the TMM within a MATLAB framework. It uses the continuity of electromagnetic fields across interfaces to model an arbitrary number of layers that make up a multilayer optical system allowing for rapid determination of reflectance spectral variations caused by RI changes in the sensor region. The effectiveness of the TMM for comparison of theoretical results with simulated data is also enhanced as a result of its ability to efficiently model planar multilayer systems. All the layers are stacked along the z-axis. The dielectric constant, the thickness of the layers $d_k$ and the RI of the $k^{th}$ layer is all defined. The transverse components of the magnetic field at the interface between the first and Nth layers are $S_1$ and $S_{N-1}$,whereas the tangential components of the electric field at the boundary between the first and Nth layers are $R_1$ and $R_{N-1}$, respectively [15, 18].

$$\begin{bmatrix} R_1 \\ S_1 \end{bmatrix} = M \begin{bmatrix} R_{N-1} \\ S_{N-1} \end{bmatrix} \tag{2}$$

Here, $R_1$ and $S_1$ specifies the electric and magnetic components, respectively, at the initial boundary. $R_{N-1}$ and $S_{N-1}$ shows similar components for the last boundary. In the case of TM-mode polarized light, it has been found that the transfer matrix can be expressed by [23]:

$$M_{ij} = \left( \prod_{k=2}^{N-1} M_k \right)_{ij}, \qquad i, j = 1, 2 \tag{3}$$

© Ariston Publications 2026. All rights reserved.

**Table 1.** Specifications of the layers used at 633 nm for the proposed sensor.

| LayerStack | Layer-1 | Layer-2 | Layer-3 | Layer-4 | Layer-5 |
|---|---|---|---|---|---|
| Material | 2S2GPrism | Cytop | ITO | $TiO_2$ | SensingMedium |
| Thickness | Semi-infinite | 2500nm | 500nm | 5nm | Semi-infinite |
| RI | 2.358 | 1.34 | 1.858+i*0.058 | 2.5837 | 1.33+Δn |
| Reference | [19] | [20] | [21] | [22] | – |

$$M_k = \begin{bmatrix} W_{11} & W_{12} \\ W_{21} & W_{22} \end{bmatrix} = \begin{bmatrix} \cos\beta_k & \frac{-i\sin\beta_k}{q_k} \\ -iq_k\sin\beta_k & \cos\beta_k \end{bmatrix} \quad (4)$$

The $\beta_k$ is the optical admittance and $q_k$ denotes the phase factor. The reflection coefficient expression for the p-polarized light may be observed by [24]:

$$r_p = \frac{(M_{11} + M_{12}q_N)q_1 - (M_{21} + M_{22}q_N)}{(M_{11} + M_{12}q_N)q_1 + (M_{21} + M_{22}q_N)} \quad (5)$$

Finally, reflected intensity is calculated as follows[25]

$$R_p = |r_p|^2 \quad (6)$$

## 3. MATLAB SIMULATION BASED RESULTS WITH ITS DISCUSSIONS

The simulated results with both TE and TM mode shown in this section. The proposed sensor's performance was also evaluated in the wide 1.33 to 1.41 RI range.

### 3.1 LMR response with dependency of polarization

With Cytop=2500nm, ITO=500nm, $TiO_2$=5nm thickness, the Figure 2a and 2b reflectivity spectra were obtained for TE and TM modes keeping RI of sensing medium 1.33. A sharp resonance curve with Rmin almost zero was obtained for TE mode when compared to TM mode. TM mode produces sallower with broader resonance curve with higher Rmin value. Although same resonance angle observed for both the modes, but still TE indicates high suitability for its applicability in LMR sensing.

### 3.2 Effect of Varying Cytop thickness

Figure 3a and 3b illustrates the angular reflectance

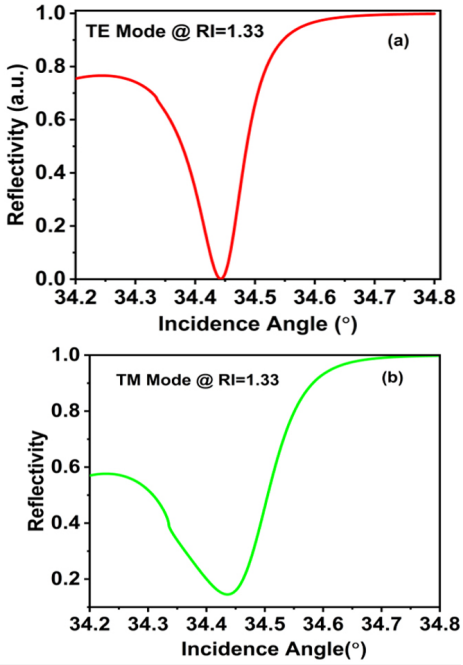



**Fig. 2.** Reflective response observed at RI=1.33 (a) TE and (b) TM mode.

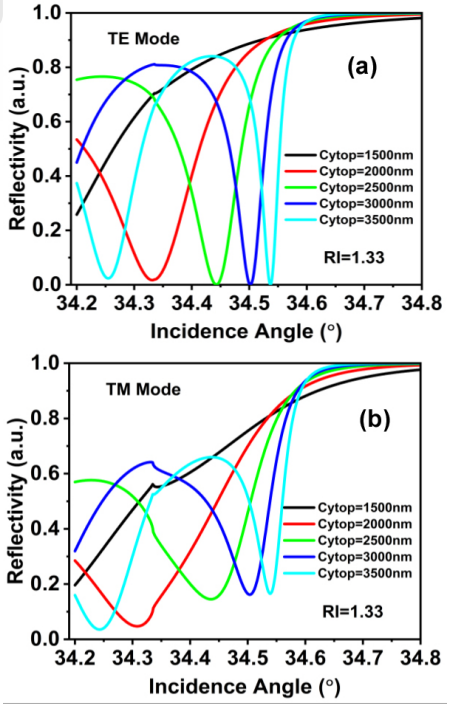



**Fig. 3.** Reflectance spectra observed for different cytop thickness for (a) TE and (b) TM modes.


© Ariston Publications 2026. All rights reserved.

characteristics of the 2S2G prism/Cytop/ITO/$TiO_2$ multi-layer LMR sensor for cytop thicknesses of 1500 to 3500 nm for TE and TM modes respectively. BK7 is the optical coupling prism, cytop is the low-index match coating, and ITO is the lossy thin-film (responsible for exciting LMR). The $TiO_2$ layer has an effect on the modal index and electric-field distributions at the sensing surface. The minima of reflectance seen in the angular spectra occur when the LMRs are excited; these occur when the propagation constant of a lossy waveguide mode satisfies the phase matching condition with incident illumination.

The optical path length and degree of modal confinement in the multi-layer structure change as the cytop thickness increases; thus, the LMR resonance angle moves from 34.33° to 34.54° while the resonance depth and line-width will vary. These variations show that cytop thickness affects phase matching, field confinement, and the coupling efficiency of the LMR mode. The RI of the sensing medium considered is 1.33.

### 3.3 Effect of varying ITO thickness

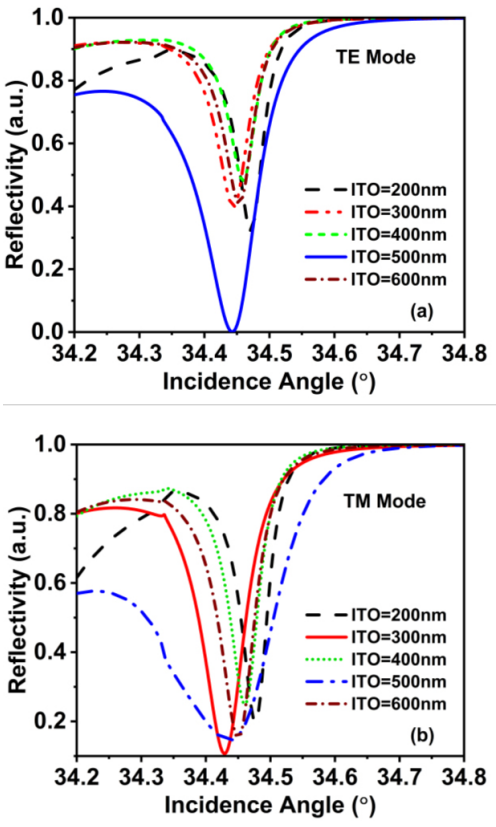



**Fig. 4.** Reflectance spectra observed for different ITO thickness for (a) TE and (b) TM modes.

Figure 4a and 4b shows the LMR sensor's reflectivity response to different ITO layer thickness variations from 200 to 600 nm, when using both TE and TM polarized light. A variety of parameters relating to the resonance characteristics are affected by the ITO layer thicknesses as well. These results indicate that the ITO layer is an important factor in the design and operation of the LMR sensor because it can be used to optimize its performance. For TE mode for 500 nm and for TM mode 300 nm, the Rmin values are the lowest.

The influence of ITO layer's thickness on SPR performance was studied by means of minimum reflectivity values (minimum Rmin), FWHM and DA for both TE and TM polarization states shown with the help of Table 2. For TE-polarization state the thinnest ITO-layer (400 nm) showed the smallest FWHM value of 0.01, and therefore the best detection accuracy of 100°-1. However, this ITO-layer shows the greatest Rmin value of 0.4819. On the other hand, the ITO-layer of 500 nm thickness provides the deepest TE-polarization resonance with a very small Rmin value of 0.00092, which is caused by a larger FWHM value of 0.03°, resulting in a smaller DA value of 33.33°-1. In case of TM-polarization state the 300 nm thick ITO layer provides the smallest Rmin value of 0.1071, thus providing the largest resonance depth, but it has the largest FWHM value of 0.07 as well. As a result, it has the smallest DA value of 14.28°-1. The largest TM-polarization DA value of 25 were obtained for the three ITO-layers with thicknesses of 200 nm, 400 nm, and 600 nm, all of them have similar FWHM values of 0.04°. Thus, we conclude that for maximal detection accuracy in TE-polarization mode the 400 nm ITO-layer should be used. If one wants to achieve the largest possible resonance depths in TE- or TM-polarization modes then either 500 nm or 300 nm thick ITO-layers could be chosen.

### 3.4 Effect of varying $TiO_2$ thickness

The influence of the thickness of $TiO_2$ layer on the optical properties of the suggested 2S2G Prism/Cytop/ITO/$TiO_2$/Sensing medium structure is shown through changing $TiO_2$ layer thicknesses from 5 to 20 nm. Reflectance spectra for both TE and TM polarization states at different thickness of $TiO_2$ layers are demonstrated in Figure 5a and 5b. A great influence is found due to modification in $TiO_2$ layer thickness, as it modifies the effective optical thickness and mode coupling conditions of the layers Cytop/ITO/ $TiO_2$. For the case of TE state, an increase in $TiO_2$ layer thickness will cause shift of the resonant angle towards higher values. In addition, narrowing of the resonant peak occurs due to the decrease of FWHM of resonant peak; from $0.11^0$ for 5 nm thick $TiO_2$ layer to $0.05^0$ for 20 nm

© Ariston Publications 2026. All rights reserved.

**Table 2.** $R_{min}$, FWHM and DA observed for varying ITO thickness for TE and TM modes.

| ITO Thickness (nm) | Rmin (TE Mode) | Rmin (TM Mode) | FWHM (TE Mode) | FWHM (TM Mode) | DA (TE Mode) | DA (TM Mode) |
|---|---|---|---|---|---|---|
| 200 | 0.3232 | 0.1983 | 0.03 | 0.04 | 33.33 | 25.00 |
| 300 | 0.3983 | 0.1071 | 0.03 | 0.07 | 33.33 | 14.28 |
| 400 | 0.4819 | 0.2494 | 0.01 | 0.04 | 100.00 | 25.00 |
| 500 | 0.00092 | 0.1453 | 0.03 | 0.19 | 33.33 | 5.26 |
| 600 | 0.4088 | 0.1508 | 0.03 | 0.04 | 33.33 | 25.00 |

thick $TiO_2$ layer. As a result of this narrowing of the resonant peaks, the degree of detection improves from $9.09^{0-1}$ to $20^{0-1}$.

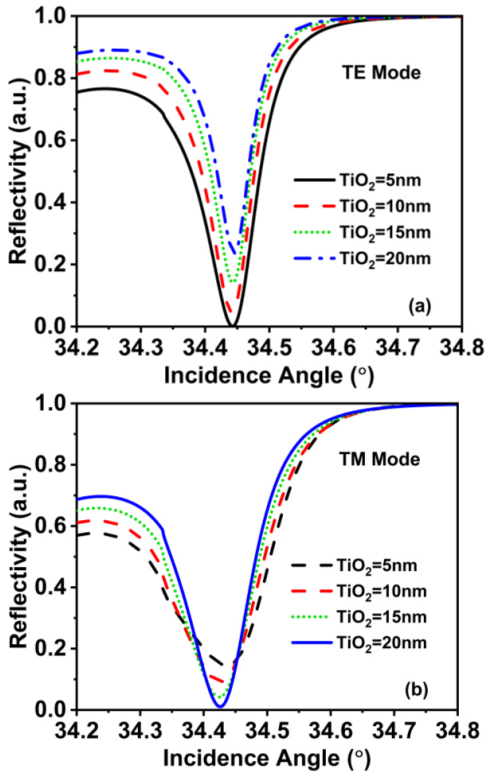



**Fig. 5.** Reflectance spectra observed for altering $TiO_2$ thickness from 5 to 20nm for (a) TE and (b) TM modes.

For TM state, increase in $TiO_2$ layer thickness causes an increase in depth of resonant minima with decreasing value of Rmin; from 0.1453 to 0.01064. Correspondingly, decrease in value of FWHM also occur; from $0.19^0$ to $0.13^0$. Hence, the DA improves from 5.26 to $7.69^{0-1}$. The data presented in Table 3 show that there are various options to modify the LMR by varying the thickness of $TiO_2$. Increasing the thickness of $TiO_2$ will result in sharper LMR peaks however based on the data provided the best option is the 5nm thick layer as it produces the strongest and most defined LMR signal (deepest minimum) and therefore has been selected as the optimal configuration for future development of Prism/Cytop/ITO/$TiO_2$/SM.

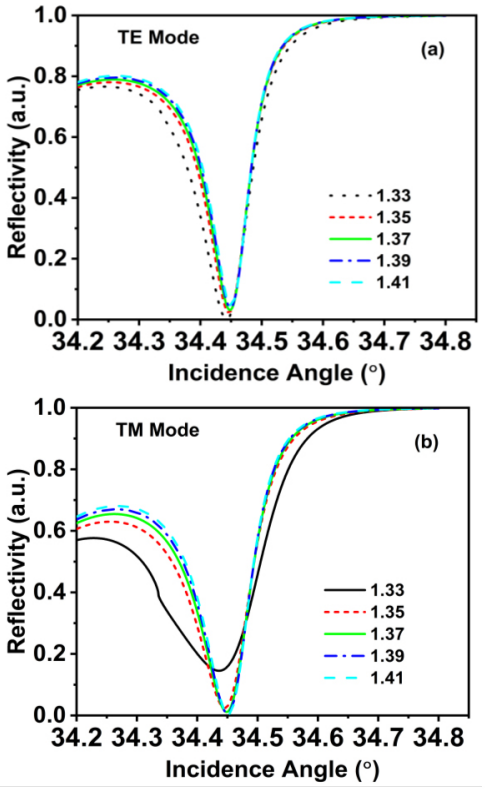



**Fig. 6.** Spectral reflectivity response (a) TE and (b) TM mode at wide RI range 1.33-1.41.

**Table 3.** $R_{min}$, FWHM and DA observed for varying $TiO_2$ thickness for TE and TM modes.

| $TiO_2$ Thickness (nm) | $R_{min}$ (TE Mode) | $R_{min}$ (TM Mode) | FWHM (TE Mode) | FWHM (TM Mode) | DA (TE Mode) | DA (TM Mode) |
|---|---|---|---|---|---|---|
| 5 | 0.0009157 | 0.1453 | 0.11 | 0.19 | 9.09 | 5.26 |
| 10 | 0.0476 | 0.0915 | 0.09 | 0.18 | 11.11 | 5.55 |
| 15 | 0.1413 | 0.0421 | 0.06 | 0.15 | 16.66 | 6.67 |
| 20 | 0.236 | 0.01064 | 0.05 | 0.13 | 20.00 | 7.69 |


© Ariston Publications 2026. All rights reserved.

### 3.5 Proposed sensor application at wide RI range

Figure 6, the spectral reflectivity graph shows surface wave resonant behavior for both TE and TM modes throughout a RI range from 1.33 to 1.41. The RI range spans common aqueous media, biological fluid systems, and many organic solvents.

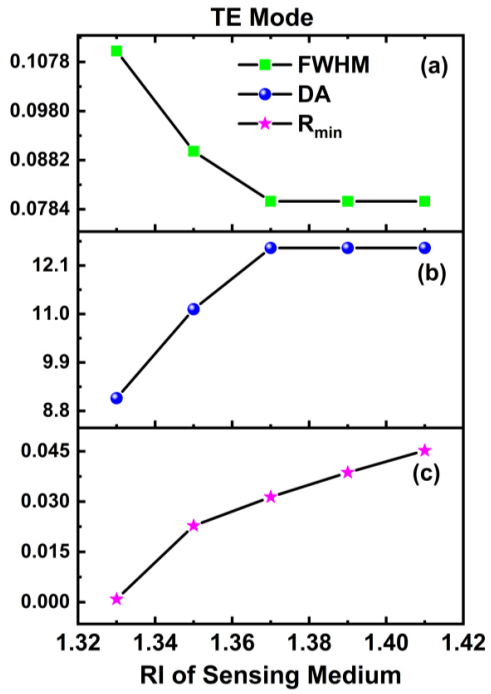



**Fig. 7.** Parameters evaluated: (a) FWHM, (b) DA and (c) Rmin for TE mode.

With an increase in the RI of the sensing medium, both polarizations (TE and TM) have a similar rightward shift in the resonant angle at approximately $\theta_r$=34.45° with slight differences in dip amplitude and line shape-most notably evident in the TM mode, as the minimum reflectivity rapidly approaches zero as the RI of the sensing medium is increased beyond 1.35. Together, the complementary responses of the TE and TM polarizations within this wide refractive index range make this optical sensor suitable for integration into lab-on-a-chip systems for biosensing and chemical diagnostic applications. The dynamic range of this sensor system provides dual-mode measurements of biological binding events (e.g., antibody-antigen interactions or DNA hybridization at approximately ns = 1.33 to 1.35 while providing simultaneous measurements of higher-RI liquids such as glucose concentration, protein solution purity, and food-quality indicators up to ns = 1.41.

The combined use of both TE and TM polarizations enhances the accuracy of sensing through cross-polarized state referencing and enables the mitigation of thermal drifts, allowing for continuous monitoring in medical, environmental, and food processing applications.

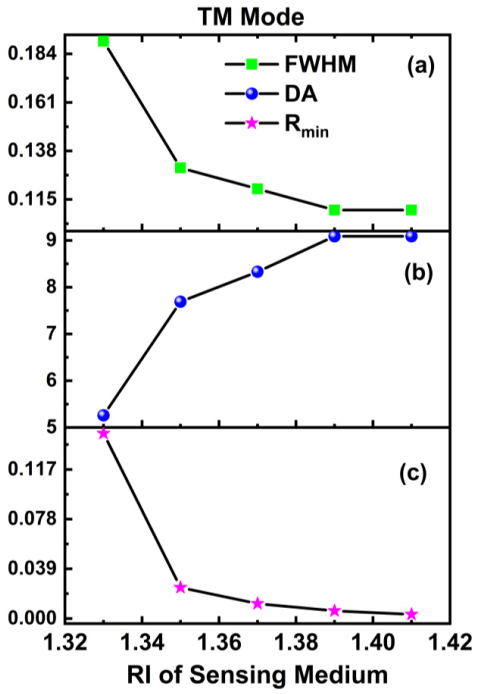



**Fig. 8.** Parameters evaluated: (a) FWHM, (b) DA and (c) Rmin for TM mode.

The performance of the LMR sensor is compared in the Table 4 for TE and TM polarized light for various refractive indices. As the RI for TE polarized light increases from 1.33 to 1.41, the FWHM, which represents how wide or narrow the peak is, decreases by approximately 0.03 and the DA increases by about 3.42.

**Table 4.** TE and TM mode performance matrix for RI ranging from 1.33 to 1.41.

| TE Mode | | | | |
|---|---|---|---|---|
| **RI** | **FWHM** | **DA** | **$R_{min}$ (a.u.)** | **$\theta$ (deg)** |
| 1.33 | 0.11 | 9.09 | 0.00091 | 34.44 |
| 1.35 | 0.09 | 11.11 | 0.02279 | 34.45 |
| 1.37 | 0.08 | 12.50 | 0.03139 | 34.45 |
| 1.39 | 0.08 | 12.50 | 0.03867 | 34.45 |
| 1.41 | 0.08 | 12.50 | 0.0452 | 34.45 |
| **TM Mode** | | | | |
| **RI** | **FWHM** | **DA** | **$R_{min}$ (a.u.)** | **$\theta$ (deg)** |
| 1.33 | 0.19 | 5.26 | 0.1453 | 34.44 |
| 1.35 | 0.13 | 7.69 | 0.0243 | 34.45 |
| 1.37 | 0.12 | 8.33 | 0.01164 | 34.45 |
| 1.39 | 0.11 | 9.09 | 0.00606 | 34.45 |
| 1.41 | 0.11 | 9.09 | 0.00321 | 34.45 |

The lowest FWHM value obtained was 0.08 with peak DA of 12.50. With this increase in the refractive index, the resonance angle remains virtually unchanged (i.e., 34.44-34.45 degrees). Similar results are observed when increasing the

© Ariston Publications 2026. All rights reserved.

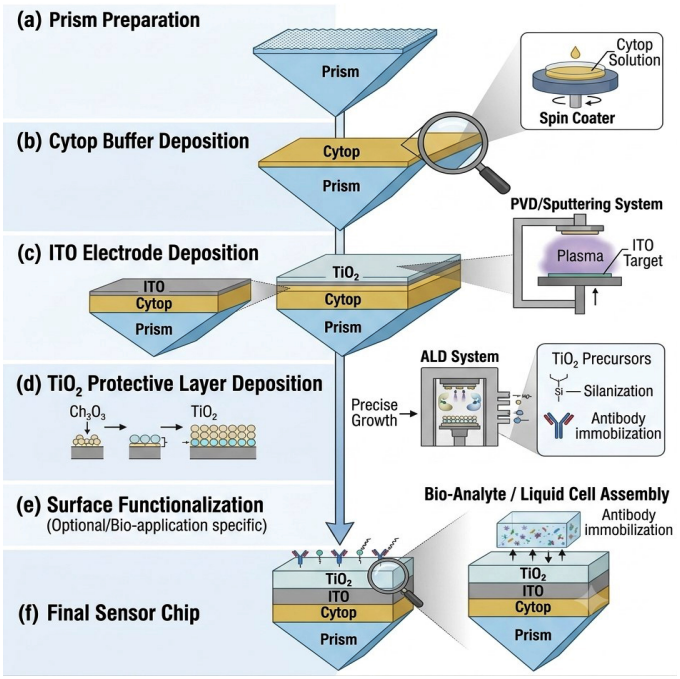



**Fig. 9.** Fabrication feasibility of presented LMR sensor.

refractive index from 1.33 to 1.41 for TM-polarized light. In addition, FWHM decreases from 0.19 to 0.11°; a noticeable enhancement in the DA value from 5.26 to 9.09°$^{-1}$ was also observed. These results show that TE-polarized light has a narrower resonance and provides greater DA than TM-polarized light, therefore providing superior total performance for the proposed LMR sensor. Table 4 shows these parameters (FWHM, $R_{min}$, $\theta_r$ and DA values).

Figure 7 and 8 presents the variation in FWHM, DA, and $R_{min}$ as a function of RI; it can be seen that the TE mode has a narrower resonant profile, better DA than the TM mode, and therefore has better sensing performance than TM.

## 4. FABRICATION FEASIBILITY OF THE PROPOSED LMR SENSOR CHIP

The feasibility of creating this 2S2G/Cytop/ITO/$TiO_2$ layering structure shown by Figure 9 is practical due to each layer being created using common thin-film processing techniques. $TiO_2$ and ITO are commonly deposited on surfaces via sputtering or pulsed-laser-deposition methods with good optical properties. Cytop is also easily spin-coated onto a surface, forming a smooth, low-index polymer film. Similarly, 2S2G is easily formed into a dielectric using thermal evaporation or sputtering methods. Due to the small tolerance for fabrication errors (e.g., the amount of material used to form the individual films) that may affect either the film's thickness or its refractive index, will likely not interfere with achieving resonance. Therefore, with common surface treatment and packaging methods available to address the issue of film adhesion and long-term stability, this new design can be built and tested using standard cleanroom equipment and can be incorporated into existing planar or fiber-optic SPR-based systems.

## 5. CONCLUSION

A numerical study of an ITO-based prism-coupled LMR sensor was carried out by applying the transfer matrix method to a structure consisting of 2S2G Prism/Cytop/ITO/$TiO_2$/Sensing medium in order to understand how varying polarization, cytop film thickness, ITO film thickness and $TiO_2$ film thickness will affect the LMR characteristics under angular interrogation. The research showed that this multi-layered structure can be used to generate LMR signals and also to provide large changes in reflectivity when changing the refractive index from 1.33 to 1.41. It was found that there are significant differences in the behaviour of the two polarization states (TE and TM), where the TE state had a deeper resonance and was thus more sensitive than the TM state. It was also observed that changing the ITO film thickness affected both the resonance intensity and detection accuracy, where films at 500nm gave the largest resonance depth. In addition, it was found that the $TiO_2$ thickness greatly influenced

 © Ariston Publications 2026. All rights reserved.

the width of the resonance and the amount of energy coupled into the waveguide. While thicker $TiO_2$ layers produced narrower resonance profiles, thinner $TiO_2$ layers provided stronger resonance signals; as such, a 5 nm thick $TiO_2$ layer provided the best-defined resonance and was chosen as the optimal configuration for this application.

## DECLARATIONS

### Ethical Approval

We affirm that this manuscript is an original work, has not been previously published, and is not currently under consideration for publication in any other journal or conference proceedings. All authors have reviewed and approved the manuscript, and the order of authorship has been mutually agreed upon.

### Funding

There are no funding

### Availability of data and material

All of the data obtained or analyzed during this study is included in the report that was submitted.

### Conflicts of Interest

The authors declare that they have no financial or personal interests that could have influenced the research and findings presented in this paper. The authors alone are responsible for the content and writing of this article.

### Author's Contributions

**A. U.:** Conceptualization (equal), Writing - review and editing (equal), Supervision (lead), **V.S.:** Writing - review and editing (equal), **P.D.U:** review and editing (equal),**D.K.D:** Supervision, review (equal). All authors have read and agreed to the published version of the manuscript.

## REFERENCES

[1] Arregui, F. J. and others, **2014**. Fiber-Optic Lossy Mode Resonance Sensors. *Procedia Engineering*, 87, p.3-8. https://doi.org/10.1016/j.proeng.2014.11.253.

[2] Mohankumar, P. and Ajayan, J. and Mohanraj, T. and Yasodharan, R., **2021**. Recent Developments in Biosensors for Healthcare and Biomedical Applications: A Review. *Measurement*, 167(May 2020), p.108293. https://doi.org/10.1016/j.measurement.2020.108293.

[3] Yesudasu, V. and Pradhan, H. S. and Pandya, R. J., **2021**. Recent Progress in Surface Plasmon Resonance Based Sensors: A Comprehensive Review. *Heliyon*, 7(3), p.e06321. https://doi.org/10.1016/j.heliyon.2021.e06321.

[4] Bijalwan, A. and Uniyal, A. and Yadav, R. B. and Alsubaie, A. and Mahmoud, K. H. and Pal, A., **2024**. Enhanced Sensing: E7-Liquid Crystal-Based Surface Plasmon Temperature Sensor with Angle Interrogation. *Plasmonics*, p.1-8.

[5] Dwivedi, A. K. and Srivastava, A. and Tripathi, S., **2022**. Tin Di-Selenide and Zinc Oxide Based SPR Biosensor for Detection of DNA Hybridization, Anemia and Abnormality in Urine. *Optical and Quantum Electronics*, 54(6), p.1-13. https://doi.org/10.1007/s11082-022-03759-9.

[6] Paliwal, N. and John, J., **2015**. Lossy Mode Resonance (LMR) Based Fiber Optic Sensors: A Review. *IEEE Sensors Journal*, 15(10), p.5361-5371.

[7] Del Villar, I. and others, **2017**. Optical Sensors Based on Lossy-Mode Resonances. *Sensors and Actuators B: Chemical*, 240, p.174-185. https://doi.org/10.1016/j.snb.2016.08.126.

[8] Szymanski, M. and Kosiel, K. and Huk, R. and Gajowniczek, K., **2024**. LMR: A Software for Modeling and Reverse Optimization of Straight-Core Lossy Mode Resonance (LMR) Based Sensors. *Expert Systems with Applications*, 251, p.123925.

[9] Martinez, E. E. G. and Hualde-Otamendi, M. and Zamarreno, C. R. and Matias, I. R., **2023**. LMR-Based Optical Sensor for Ethylene Detection at Visible and Mid-Infrared Regions. *IEEE Sensors Letters*, 7(8), p.1-4.

[10] Rivero, P. J. and Urrutia, A. and Goicoechea, J. and Matias, I. R. and Arregui, F. J., **2013**. A Lossy Mode Resonance Optical Sensor Using Silver Nanoparticles-Loaded Films for Monitoring Human Breathing. *Sensors and Actuators B: Chemical*, 187, p.40-44.

[11] Saini, R. and others, **2019**. Lossy Mode Resonance-Based Refractive Index Sensor for Sucrose Concentration Measurement. *IEEE Sensors Journal*, 20(3), p.1217-1222.

© Ariston Publications 2026. All rights reserved.

[12] Del Villar, I. and Zamarreno, C. R. and Hernaez, M. and Arregui, F. J. and Matias, I. R., **2010**. Generation of Lossy Mode Resonances with Absorbing Thin-Films. *Journal of Lightwave Technology*, 28(23), p.3351-3357.

[13] Zamarreno, C. R. and Hernaez, M. and Del Villar, I. and Matias, I. R. and Arregui, F. J., **2010**. ITO Coated Optical Fiber Refractometers Based on Resonances in the Infrared Region. *IEEE Sensors Journal*, 10(2), p.365-366.

[14] Paliwal, N. and John, J., **2014**. Theoretical Modelling of Lossy Mode Resonance (LMR) Based Fiber Optic Temperature Sensor Utilizing TiO2 Sensing Layer. *International Conference on Fibre Optics and Photonics*, p.M4A-22.

[15] Zaman, M. U. and others, **2025**. Plasmonic Sensing of Human Teeth: A Molybdenum Ditelluride-Black Phosphorus-Based Surface Plasmon Resonance Approach. *Plasmonics*, p.1-13.

[16] Del Villar, I. and Zamarreno, C. R. and Hernaez, M. and Arregui, F. J. and Matias, I. R., **2010**. Lossy Mode Resonance Generation with Indium-Tin-Oxide-Coated Optical Fibers for Sensing Applications. *Journal of Lightwave Technology*, 28(1), p.111-117. https://doi.org/10.1109/JLT.2009.2036580.

[17] Wu, L. and others, **2018**. High-Performance Lossy-Mode Resonance Sensor Based on Few-Layer Black Phosphorus. *The Journal of Physical Chemistry C*, 122(13), p.7368-7373. https://doi.org/10.1021/acs.jpcc.7b12549.

[18] Pal, A. and others, **2025**. Simulation-Based Study of a Novel SPR Sensor Employing Cadmium Sulfide and Carbon Nanotubes. *Plasmonics*, p.1-12.

[19] Karki, B. and Uniyal, A. and Srivastava, G. and Pal, A., **2023**. Black Phosphorous and Cytop Nanofilm-Based Long-Range SPR Sensor with Enhanced Quality Factor. *Journal of Sensors*, 2023, p.2102915. https://doi.org/10.1155/2023/2102915.

[20] Wu, L. and Che, K. and Xiang, Y. and Qin, Y., **2022**. Enhancement of Sensitivity with High-Reflective-Index Guided-Wave Nanomaterials for a Long-Range Surface Plasmon Resonance Sensor. *Nanomaterials*, 12(168).

[21] Han, L. and Chen, Z. and Huang, T. and Ding, H. and Wu, C., **2020**. Sensitivity Enhancement of Ag-ITO-TMDCs-Graphene Nanostructure Based on Surface Plasmon Resonance Biosensors. *Plasmonics*, 15(3), p.693-701. https://doi.org/10.1007/s11468-019-01079-5.

[22] Taya, S. A. and others, **2023**. Highly Sensitive Sensor Based on SPR Nanostructure Employing Graphene and Perovskite Layers for the Determination of Blood Hemoglobin Concentration. *Optik*, 281(November 2022), p.170857. https://doi.org/10.1016/j.ijleo.2023.170857.

[23] Sarkar, P. and others, **2026**. Sensitivity Tuning of SPR Sensor for the Detection of Water Pollutants Using Black Phosphorus and CeF3. *Journal of Computational Electronics*, 25(3), p.111.

[24] Dixit, G. and Sharma, V. and Dwivedi, L. K. and Singh, S. and Nigam, S. K. and Uniyal, A., **2026**. Numerical Study of Gallium Nitride and Lead Titanate-Based SPR Sensor for HIV Detection in Human Blood. *Sensing and Imaging*, 27(1), p.93.

 © Ariston Publications 2026. All rights reserved.